This is the accepted manuscript made available via CHORUS. The article has been published as:

Screening confinement of entanglements: Role of a self-propelling end inducing ballistic chain reptation

Xue-Zheng Cao, Holger Merlitz, Chen-Xu Wu, and M. Gregory Forest

Phys. Rev. E **106**, L022501 — Published 9 August 2022

DOI: 10.1103/PhysRevE.106.L022501

Self-Propelling End Induces Ballistic Chain Reptation to Screen Confinement of Entanglements

Xue-Zheng Cao,[1,*] Holger Merlitz,[2] Chen-Xu Wu,[1] and M. Gregory Forest[3]

[1]*Department of Physics, Xiamen University, Xiamen 361005, P.R. China*
[2]*Leibniz-Institut für Polymerforschung Dresden, 01069 Dresden, Germany*
[3]*Departments of Mathematics, Applied Physical Sciences, Biomedical Engineering, University of North Carolina at Chapel Hill, Chapel Hill, NC 27599-3250, United States*

(Dated: July 18, 2022)

Synthetic and natural nanomaterials with self-propelling mechanisms continue to be explored to boost chain mobility beyond normal reptation in the crowded environments of entangled chains. Here we employ scaling theory and numerical simulations to demonstrate that activating one chain end of a singular or isolated chain boosts entanglement-constrained chain reptation from the one-dimensional diffusive mobility as described by the deGennes-Edwards-Doi model to ballistic motion along the entanglement tube contour. The active chain is effectively screened from the constraint of entanglements on length scales exceeding the tube size.

Entanglements suppressing chain motion is an important microscopic origin that determine the rheological properties of many materials composed of long polymer chains [1, 2]. A regulation of dynamical mechanic properties of related polymer materials requires a manipulation of the dynamics of individual chains, which is limited by entanglements. Releasing long chains from entanglement constraints to achieve enhanced chain mobility is a challenge in polymer physics and soft matter, whose solution has a wide range of biomedical and industrial applications [3–18]. Growing examples of synthetic and natural systems, e.g., nano-motors and biological microswimmers, with self-propelling characteristics, inspire the possibility to manipulate the relaxation dynamics of entangled polymer chains by giving selected chain segments the ability to self-propel [19–30]. Here we explore and report results for local activation of the end of a single isolated chain within an otherwise passive entangled polymer chain melt, showing that the active chain effectively screens confinement of the surrounding entanglements via taking ballistic reptation to release along the entanglement tube.

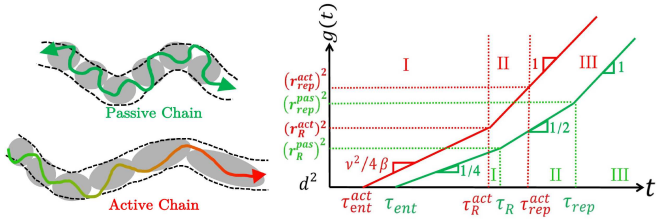


FIG. 1. (color online). Left panel: Sketches showing the reptation motions of active and passive chains along the entanglement tube. We mark both ends of the passive chain as green arrows to indicate their identical mobility, while the active chain is marked as being oriented by a red arrow, with the red-to-green color contour change representing the decreasing influence of the self-propelling end on the stretching of chain segments closer to the passive end. Right panel: Scaling predictions of mean squared displacements (MSDs), for the self-propelling end (shown in red lines) based on the theoretical discussions proposed in the present paper, and for a passive chain end (shown in green lines) based on the de-Gennes-Edwards-Doi model. The dashed lines are shown to separate different scaling regimes.

Based on the tube model proposed by de Gennes, Edwards, and Doi, see Figure 1, there exist three regimes that commence once the tube confinement of entanglements starts to take effect, namely beyond the critical timescale, $\tau_{\rm ent}$. The mean squared displacement $g(t) =< \Delta\mathbf{r}^2(t) >$ of a monomer belonging to an entangled network of passive, ideal polymer chains exhibits [31]: (I) A subdiffusive regime related to the confinement-induced one dimensional Rouse relaxation of entanglement blobs, $g(t) \sim t^{1/4}$ when $\tau_{\rm ent} < t < \tau_{\rm R}$, with $\tau_{\rm R}$ being the Rouse time at which the whole chain begins to move coherently along the tube contour; (II) another subdiffusive regime related to the one-dimensional random motion reptation of the whole chain along the entanglement tube, $g(t) \sim t^{1/2}$ when $\tau_{\rm R} < t < \tau_{\rm rep}$, where $\tau_{\rm rep}$ is the critical timescale from which the chain becomes completely relaxed from the original confinement of entanglements; and (III) the regime of Fickian diffusion, $g(t) \sim t$ when $t > \tau_{\rm rep}$. Note that, the de-Gennes-Edwards-Doi model was built by regarding polymer chains as ideal and assuming that all monomers of an entangled chain are constrained identically by surrounding polymer chains that form a stable entanglement tube. This mechanism contributes to the scaling exponents for experimental and simulated entangled polymers, as confirmed in previous simulations to exhibit deviations from the theoretical predictions of the de-Gennes-Edwards-Doi model. This arises in particular for the MSD of monomers close to chain ends [32, 33].

For an entangled single active chain, the effective temperature $T^{\rm act}$ of the self-propelling end is higher than the thermal $T^{\rm pas}$ of the remaining (passive) monomers that belong to the chain. Therefore, the self-propelling end stretches adjacent chain segments before they have been given sufficient time to complete their structural relaxation through conventional thermal motion. Since the segment's size is enlarged by the stretching, we assume a scaling dependence of the mean square end-to-end distance and a corresponding time dependent scaling exponent, yielding

$$< r_{ete}^2[N(t)] > \sim N^{\nu(t)}(t), \qquad (1)$$

with $\nu(t) > 1$, in which $N(t)$ is the number of monomers adjacent to the self-propelling end that are affected by the active monomer at a time t. Note that the stretching effect degener-

ates as $N(t)$ increases, yielding a gradually decreasing value of $\nu(t)$, which approaches unity as time evolves.

The time-dependent diffusion coefficient and the corresponding displacement for the self-propelling end, at small timescales, can be approximately defined as $D_{\rm act}(t) \approx \frac{kT^{\rm act}}{N(t)\zeta_{\rm m}}$ and $g(t) = 6\frac{kT^{\rm act}}{N(t)\zeta_{\rm m}}t$, respectively, with $\zeta_{\rm m}$ being the monomeric friction coefficient. Entanglements of surrounding polymer chains start to confine the motion of a monomer when its mean square displacement $g(t) > d^2$, where d is the entanglement tube size formed by surrounding chains of the polymer melt, regardless whether the single chain is active or passive. Therefore, the critical timescale, at which the monomer's motion begins to be confined by entanglement, shifts from $\tau_{\rm ent}^{\rm pas} \sim \frac{N_{\rm ent}\zeta_{\rm m}d^2}{kT}$ for an end of one passive chain, to $\tau_{\rm ent}^{\rm act} \sim \frac{N(\tau_{\rm ent}^{\rm act})\zeta_{\rm m}d^2}{kT^{\rm act}}$ for the self-propelling end of an active chain. According to Eq.(1), a lower number of monomers is required in the stretched active chain segment than in a passive one to make the segment's end-to-end distance comparable with the entanglement tube size, thus $N(\tau_{\rm ent}^{\rm act}) < N_{\rm ent}$. In addition, because of $T^{\rm act} > T^{\rm pas}$, $\tau_{\rm ent}^{\rm act} < \tau_{\rm ent}^{\rm pas}$ is expected to hold, indicating an earlier onset of the entanglement related confinement to take effect.

After $t = \tau_{\rm ent}^{\rm act}$, the confinement of entanglements induced by surrounding polymer chains prevents any coherent chain motion transverse to the entanglement tube over length scales exceeding the entanglement length, and the active chain is restricted to movements along the entanglement tube. As time evolves, an increasing number of monomers in the active chain participates in the motion driven by the self-propelling end. As with the confined motion of the passive chain along its entanglement tube, there exists a critical timescale, $\tau_{\rm R}^{\rm act}$ that determines at which point all monomers in the active chain participate in the motion of its active end. As shown in Figure 1, the active chain relaxation, over timescales of $\tau_{\rm ent}^{\rm act} < t < \tau_{\rm R}^{\rm act}$, can be regarded as the relaxation of a chain consisting of stretched entanglement blobs. Along the contour of the entanglement tube, blobs closer to the self-propelling end are stretched out further and participate earlier in the self-propelling end's coherent motion. Therefore, we assume there exists a scaling dependence of the relaxation time of a chain section on the number of involved entanglement blobs M,

$$\tau_{\rm mb} \sim M^{2\beta({\rm t})}, \tag{2}$$

where $\beta(t) < 1$ and gradually approaching unity as time evolves and the degree of stretching diminishes. Based on Eq.(1) and Eq.(2), the one dimensional mean squared displacement along the contour of the entanglement tube then yields

$$< \Delta s^2(t) > \sim M^{\nu} \sim t^{\frac{\nu}{2\beta}}. \tag{3}$$

Moreover, the three dimensional mean squared displacement of the self-propelling end takes the form

$$g(t) \sim \left(\sqrt{< \Delta s^2(t) >}\right)^{\nu} \sim t^{\nu^2/4\beta}, \tag{4}$$

as $\tau_{\rm ent}^{\rm act} < t < \tau_{\rm R}^{\rm act}$, in which the value of $\nu^2/4\beta$ decreases with time as a result of decreasing ν and increasing β.

At timescales of $t > \tau_{\rm R}^{\rm act}$, the whole chain moves coherently to relax from the existing entanglement tube. One qualitative difference between the reptation motions of active and passive chains is that all monomers in the active chain have to move along with its self-propelling end, while there is no preferred direction in the passive chain due to the absence of a mobility imparity between the two ends. We can regard the self-propelled reptation motion along the entanglement tube as effectively ballistic, so that

$$g(t) \sim \left(\sqrt{< \Delta s^2(t) >}\right)^{\nu} \sim \left(\sqrt{D_{\rm rep}t^2}\right)^{\nu} \sim t^{\nu}, \tag{5}$$

while $\tau_{\rm R}^{\rm act} < t < \tau_{Rep}^{act}$, where $D_{\rm rep}$ is the curvilinear diffusion coefficient of the chain's center-of-mass motion along the entanglement tube, and $\tau_{\rm rep}^{\rm act}$ is the reptation time after which the active chain has fully relaxed from the constraint of the original entanglement tube. Once the active chain has completed its reptation relaxation, the active end's MSD enters its Fickian diffusion regime, in which

$$g(t) = 6D_{\rm f}t \sim t, \tag{6}$$

as $t > \tau_{\rm rep}^{\rm act}$ and $D_{\rm f}$ is the Fickian diffusion coefficient of the active chain. Note that the scaling exponent ν defined in Eq.(1) approaches unity after about $t = \tau_{\rm R}^{act}$, because the transient stretching effect induced by the self-propelling end diminishes over large timescales comparable to the Rouse time of the chain. Therefore, as shown in Figure 1, there exists no crossover in the self-propelling end's MSD from the regime of reptation motion as defined by Eq.(5) to the Fickian diffusion regime, which signifies that the confinement of entanglements is effectively screened.

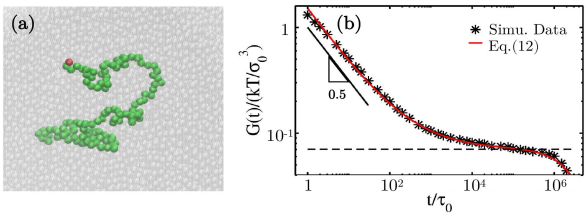


FIG. 2. (color online). The modeled system of a single chain in an entangled polymer melt. (a) A simulation snapshot showing the conformation of an active chain of $N = 128$ and bending energy parameter $\varepsilon_{\rm bend} = 0$, with its self-propelling end of driving force $f_{\rm sp} = 8$ (red). The entangled polymer melt is shown in grey. (b) Simulation result of the stress relaxation moduli of the entangled polymer melt, and the corresponding theoretical fit based on Eq.(9) with the fit parameters $n_{\rm m} = 0.80$, $\tau_{\rm mon} = 3.0$, $\gamma = 0.50$, $G_{\rm pla}^{\rm red} = 0.088$ and $\tau_{\rm ter} = 4.3 \cdot 10^6$. The dashed horizontal line indicates the plateau modulus of $G(t) = n_{\rm m}kT\,G_{\rm pla}^{\rm red}$. Here, the polymer chain length and the bending energy parameter between neighboring bonds governing the stiffness of polymer chains in the melt are $N = 256$ and $\varepsilon_{\rm bend} = 2$, respectively.

Moleclular dynamics (MD) simulations were performed to verify the systematic shift of the chain end's diffusional behavior as proposed in the above theoretical scaling model. Polymer chain is composed of Lennard-Jones (LJ) spheres representing Kuhn monomers that are connected by harmonic springs governed by a finitely extensible elastic potential, defined as

$$U_{\rm bond}(r) = k(r-\sigma_0)^2, \tag{7}$$

where $k = 100\varepsilon_0/{\sigma_m}^2$ is the spring constant, ε_0 is the energy unit, and σ_0 is the length unit. The stiffness of polymer chains is governed by defining the bending potential between every two neighboring bonds,

$$U_{\rm bend}(\theta) = \varepsilon_{\rm bend}(\theta-\pi)^2, \tag{8}$$

where θ is the angle between the two bonds. The monomer-monomer interactions were modeled as truncated and shifted Lennard-Jones (LJ) potentials

$$U_{\rm LJ}(r) = 4\varepsilon_0\left[\left(\frac{\sigma_{ij}}{r}\right)^{12} - \left(\frac{\sigma_{ij}}{r}\right)^{6} - \left(\frac{\sigma_{ij}}{r_c}\right)^{12} + \left(\frac{\sigma_{ij}}{r_c}\right)^{6}\right], r < r_c, \tag{9}$$

where $\sigma_{\rm ij} = \sigma_0$ stands for the mean size of two particles (i th and j th) involved in the pair interactions of monomer-monomer. It is easily verified that with the cutoff of, $r_{\rm c} = 2^{\frac{1}{6}}\sigma_{\rm ij}$, implemented, the attractive contribution to this potential is eliminated, i.e. $U_{\rm LJ}(r) = 0$ when $r > r_{\rm c}$.

In this work, the LJ system of units is used. It is defined using a model polymer with a LJ pair potential, featuring the length unit σ_0, the energy unit ε_0 and the mass unit m_0 as the fundamental quantities. All simulations started from an initial condition with chains of polymer melt distributed homogeneously. The boundary conditions in all three directions are periodic. The simulations are carried out at fixed cubic box size $d = 40\sigma_0$, which is much larger than the averaged radius of gyration of (polymer melt) chains of $l_{\rm c} = 256$. Figure 2(a) displays the system of a single active chain with a self-propelling end, immersed in a melt of of entangled polymer chains. In the simulation, the equation of motion for the displacement of a passive monomer of index i is given by the Langevin equation [34, 35]:

$$m_0\frac{d^2\mathbf{r}_i}{dt^2} = -\nabla U_i - \zeta\frac{d\mathbf{r}_i}{dt} + \mathbf{F}_i, \tag{10}$$

where m_0 is its mass, $\mathbf{r}_i$ its coordinate, and U_i the total conservative potential energy at this position. The quantity $\mathbf{F}_i$ is a random external force (white noise) with a second moment proportional to the temperature and the friction constant ζ. For the self-propelling end, there is an additional driving force pointing into the current direction of its velocity vector,

$$m_0\frac{d^2\mathbf{r}_{\rm act}}{dt^2} = -\nabla U_{\rm act} - \zeta\frac{d\mathbf{r}_{\rm act}}{dt} + \mathbf{F}_{\rm act} + f_{\rm sp}\mathbf{e}_v(t), \tag{11}$$

where $\mathbf{e_v(t)}$ is the unit vector of the self-propelling end's instaneous velocity at time t, and $f_{\rm sp}$ is the constant value of the driving force.

In order to reduce effects of constraint release of the surrounding polymer chains on the relaxation dynamics of a single active/passive chain, we introduce a moderate degree of chain-stiffness to establish a stably entangled matrix, whose conformations relax on time scales longer than the reptation time of the single active/passive chain. There are $\varepsilon_{\rm bend} = 2$ for the chains of polymer melt, and $\varepsilon_{\rm bend} = 0$ for the single active/passive chain, respectively. The presence of chain entanglements in the melt was confirmed by measuring the stress relaxation moduli, $G(t)$, using a Green-Kubo protocol which relates $G(t)$ to the time-dependent auto-correlation function of the off-diagonal elements of the system's stress tensor [36–38]. As shown in Figure 2(b), we adopt an empirical scaling formula with a smooth crossover between the Rouse and reptation relaxation regimes to fit the measured simulation data of $G(t)$:

$$G(t) = n_{\rm m}\cdot k_{\rm B}T\cdot\left[\left(\frac{t}{\tau_{\rm mon}}\right)^{\gamma} + G_{\rm pla}^{\rm red}\right]\cdot\exp\left(-\frac{t}{\tau_{\rm ter}}\right). \tag{12}$$

As a result, we obtain the entanglement length of the melt, $N_{\rm ent} = \frac{1}{G_{\rm pla}^{\rm red}} \approx 11$, i.e. about 11 monomers form a chain strand between two neighbouring entanglements.

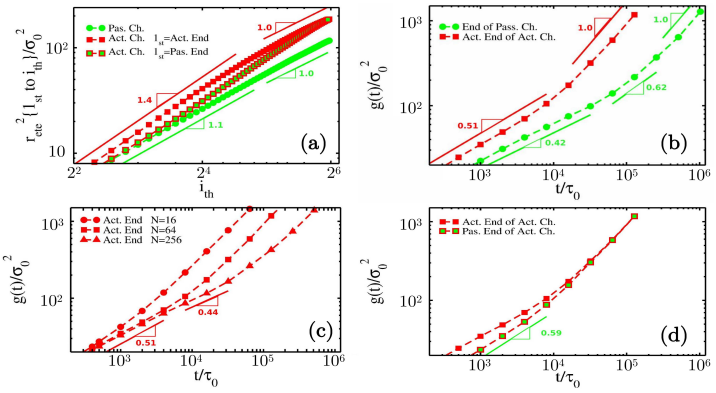


FIG. 3. (color online). Simulation results. (a) Dependence of polymer subchain size, quantified by the mean square end-to-end distance, on the subchain's chemical distance to the respective end. In case of the active chain, the active end-monomer is driven with $f_{\rm sp} = 8$ (red squares), while its second end remains passive (red-green squares). The passive chain has two passive ends (green spheres). Both chains have $N = 64$ monomers. (b) MSDs of the corresponding chain ends. (c) MSDs of the self-propelling end for different chain lengths. (d) Comparison between the MSDs of the active-and the passive ends of the same chain of length $N = 64$ and driving force $f_{\rm sp} = 8$.

Figure 3(a) displays variations of the squared end-to-end distances as a function of the segment-size, i.e. the number of monomers starting at one of the chain ends. In case of the active chain the self-propelling side (red squares) and the passive side (red-green squares) are evaluated separately. While the passive chain (green spheres) shows the familiar random walk scaling, the active chain, starting from its active end, exhibits a locally swollen chain section which further down the

chain crosses over into the ideal chain scaling, which is in line with the crossover behavior as proposed in Eq.(1). The corresponding MSD data for active and passive chain ends is shown in Figure 3(b). In case of the passive chain, the first subdiffusive regime with exponent $\gamma_{\rm pas}^{\rm ent} = 0.42$ gradually crosses over to the reptation regime of $\gamma_{\rm pas}^{\rm rp} = 0.62$, before it assumes linear Fickian diffusion. As clarified above, the approximation of ideal chains, made in the de-Gennes-Edwards-Doi model, which assumes a homogeneous diffusion behavior for all monomers along the whole chain, is responsible for the deviations between the theoretically predicted scaling exponent in the MSD of the passive chain end with simulations.

For the active chain, the self-propelling end's MSD crosses over from a subdiffusion regime with a scaling exponent of $\gamma_{\rm act}^{\rm sub} = 0.51$ to the Fickian diffusion regime, which confirms the theoretical discussion based on Eq.(5), i.e. no intermediate reptation regime is found. Figure 3(c) shows the MSD scaling of active chains of various chain lengths. In case of the longest chain ($N = 256$, triangles), an intermediate regime arises beyond $\tau/\tau_0 \approx 10000$ in which the scaling exponent is reduced, which demonstrates the decreasing dependence of the scaling exponent on time, as discussed along with Eq.(4). The emergence of this complex intermediate diffusion regime supports the scaling assumptions made in Eq.(1) and Eq.(2), i.e. the introduction of time-dependent scaling exponents, expressing the fact that the self-propelling end induces a chain stretch that diminishes in time while the majority of monomers join its motion. The resulting decrease of $\nu(t)$ and the corresponding increase of $\beta(t)$ with t leads to this transient regime in which the scaling exponent is dropping, and which remains invisible with the shorter chains where it falls into the crossover to the Fickian regime.

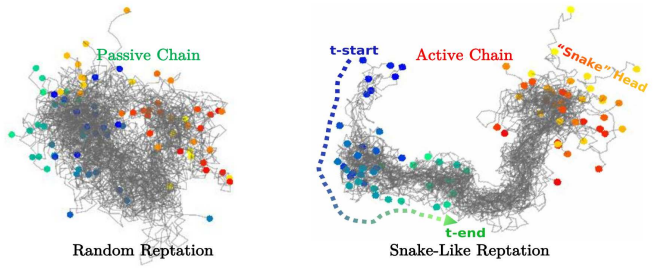


FIG. 4. Time-dependent conformational evolvements of the passive and active chains with $f_{\rm sp} = 8$ and $N = 128$. The conformations are obtained by dumping their coordinates in intervals of $10^3\tau_0$, and a total of 40 conformations is displayed for each chain. Beads are only shown at the chain ends, otherwise only the bond vectors are plotted. Time evolution is shown in terms of color changes of the chain ends: red $\rightarrow$ yellow (active end of the active chain and one arbitrary end of the passive chain) or blue $\rightarrow$ green (remaining passive ends). The dashed curve is only used for guiding the eyes.

MSDs of the self-propelling and passive ends of the active chain are compared in Figure 3(d). Due to $\zeta_{\rm m}^{\rm act} < \zeta_{\rm m}$, the passive end exhibits a slower diffusional motion than the self-propelling end on short timescales when the local stretch imposed by the self-propelling end has not yet affected the motion of the passive end, i.e. at $t < \tau_{\rm R}^{\rm act}$. Then after $t > \tau_{\rm R}^{\rm act}$, the MSD of the passive end has a larger scaling exponent than the self-propelling end, since it accelerates along with the coherent motion induced by the self-propelling end as the stretching of the chain releases. From the color-coding of the chain ends as shown in Figure 4, it is discernible that the self-propelling end's movement is followed by the passive end trailing along the entanglement tube contour, revealing that, before the active chain is fully relaxed from the confinement of entanglements, i.e. at $t < \tau_{\rm rep}^{\rm act}$, the active chain as a whole can only move directionally along the contour of the current entanglement tube. The conformational evolvement of active/passive chains confirms the theoretical scaling analysis, as concluded by Eq.(5), that the one dimensional reptation motion of the active chain along the entanglement tube is ballistic snake-like and directed toward the driven motion of the self-propelling end rather than a one-dimensional random motion. It is also visible in Figure 4 that such a ballistic chain motion with snake-like characteristics is not observed with the reptation motion of a passive chain, in which the two ends show an identical relaxation from the confinement of entanglements. A similar oriented one dimensional motion of a self-propelled end was experimentally observed by Steven Chu et al. adopting single-molecule techniques to visualize and characterise the motion and relaxation of entangled single chains with one end being attached to a microbead. In their experiments, the bead is driven by an optical tweezer and effectively acting as a self-propelling end (whose motion remains, however, restricted to a selected direction in the laboratory frame) [39].

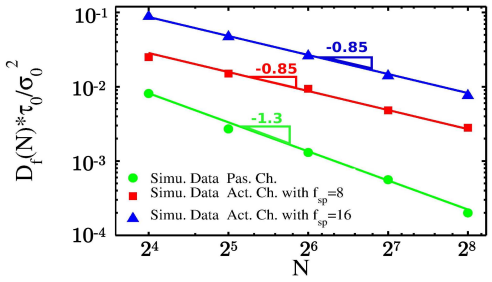


FIG. 5. (color online). Scaling dependence of the Fickian diffusion coefficients of the active (with $f_{\rm sp} = 8$ and 16) and passive chains, obtained from the MSDs of their respective ends, on the chain length. Note that the MSD curves, for the self-propelling and passive ends of the same active chain, coincide with each other in the Fickian diffusion regime as shown in Figure 3(d).

As a result of taking on a ballistic reptation motion along the entanglement tube, the active chain is effectively screened from the constraints imposed by entanglements on length-scales exceeding the entanglement tube size, which results in the scaling dependence as shown in Figure 5, where the Fickian diffusion coefficient exhibits weaker dependence on chain length than corresponding passive chains. Moreover, it is confirmed in Figure 5 that the corresponding scaling exponent in the dependence of the Fickian diffusion on chain length is in-

dependent of the driving force f_{sp} because of the unchanged mode of motion taken by the active chain once ballistic reptation is induced.

In summary, through a scaling analysis extension of the deGennes-Edwards-Doi tube model and numerical simulations, we show that a single active chain with a self-propelling end within an entangled passive polymer melt undergoes ballistic reptation in contrast with the random motion along the entanglement tube of a passive chain. Activation localized at the chain end effectively screens the active chain from entanglement constraints on passive chains. This work provides important computational and theoretial foundations for achieving boosted chain diffusion in crowded environments of entangled chains, without the need to disrupt the entanglement tube formed by surrounding polymer chains. The design of an active chain with desired distribution of self-propelling objects, that are responsive to external fields is now within reach of state of the art nanotechnology, which makes this work interesting for diverse applications ranging from transport of large molecular species (e.g., drugs) within biological membranes, or engineering strong and tough polymeric materials, to accelerated degradation of polymeric waste materials [40–50]. Furthermore, the basic mechanism of overcoming constraints imposed by entanglements is not restricted to melts but applies as well to polymer chains that are solvated in a crowded environment, in which active biological swimmers could possibly be as small as catalytic enzymes, and certain molecular motors are even smaller than that [51, 52].

Acknowledgements This research was supported in part by the National Science Foundation of China through Grants NSFC-11974291, NSFC-11974292 and NSFC-12174323. This work was also partly supported by the Fundamental Research Funds for the Central Universities (No.20720160123 and No.20720210005) and the Natural Science Foundation of Fujian Province of China (No.2020J01009), the U.S. National Science Foundation (DMS-1816630 and CISE-1931516), and the Alfred E. Sloan Foundation.

* xzcao@xmu.edu.cn

[1] M. E. D. Rosa and H. H. Winter, Rheologica Acta **33**, 220 (1994).
[2] H. Watanabe, Progress in Polymer Science **24**, 1253 (1999).
[3] G. D. Hattemer and G. Arya, Macromolecules **48**, 1240 (2015).
[4] X. Z. Cao, H. Merlitz, C. X. Wu, G. Ungar, and J. U. Sommer, Nanoscale **8**, 6964 (2016).
[5] T. B. Martin, K. Mongcopa, R. Ashkar, P. Butler, R. Krishnamoorti, and A. Jayaraman, Journal of the American Chemical Society **137**, 10624 (2015).
[6] A. C. Balazs, T. Emrick, and T. P. Russell, Science **314**, 1107 (2006).
[7] R. Mangal, S. Srivastava, and L. A. Archer, Nature Communications **6**, 7198 (2015).
[8] E. Senses, A. Faraone, and P. Akcora, Scientific Reports **6**, 29326 (2016).
[9] E. Senses, S. M. Ansar, C. L. Kitchens, Y. Mao, S. Narayanan, B. Natarajan, and A. Faraone, Physical Review Letters **118**, 147801 (2017).
[10] E. Senses, S. Narayanan, and A. Faraone, ACS Macro Lett. **8**, 558 (2019).
[11] E. Senses, S. Darvishi, M. S. Tyagi, and A. Faraone, Macromolecules **53**, 4982 (2020).
[12] E. Y. Lin, A. L. Frischknecht, and R. A. Riggleman, Macromolecules **54**, 5335 (2021).
[13] E. J. Bailey and K. I. Winey, Progress in Polymer Science **105**, 101242 (2020).
[14] H. Emamy, S. K. Kumar, and F. W. Starr, Physical Review Letters **121**, 207801 (2018).
[15] M. Abadi, M. F. Serag, and S. Habuchi, Nature Communications **9**, 5098 (2018).
[16] M. Zamponi, M. Kruteva, M. Monkenbusch, L. Willner, A. Wischnewski, I. Hoffmann, and D. Richter, Physical Review Letters **126**, 187801 (2021).
[17] I. Chubak, C. N. Likos, K. Kremer, and J. Smrek, Physical Review Research **2**, 043249 (2020).
[18] E. Locatelli, V. Bianco, and P. Malgaretti, Physical Review Letters **126**, 097801 (2021).
[19] H. D. Vuijk, H. Merlitz, M. Lang, A. Sharma, and J.-U. Sommer, Physical Review Letters **126**, 208102 (2021).
[20] S. Mandal, C. Kurzthaler, T. Franosch, and H. Löwen, Physical Review Letters **125**, 138002 (2020).
[21] S. Mukherjee, R. K. Singh, M. James, and S. S. Ray, Physical Review Letters **127**, 118001 (2021).
[22] J. Palacci, S. Sacanna, S.-H. Kim, G.-R. Yi, D. J. Pine, and P. M. Chaikin, Philosophical Transactions of the Royal Society A: Mathematical, Physical and Engineering Sciences **372**, 20130372 (2014).
[23] A. Somasundar, S. Ghosh, F. Mohajerani, L. N. Massenburg, T. Yang, P. S. Cremer, D. Velegol, and A. Sen, Nature Nanotechnology **14**, 1129 (2019).
[24] J. R. Baylis, J. H. Yeon, M. H. Thomson, A. Kazerooni, X. Wang, A. E. S. John, E. B. Lim, D. Chien, A. Lee, J. Q. Zhang, *et al.*, Science Advances **1**, e1500379 (2015).
[25] C. Bechinger, R. Di Leonardo, H. Löwen, C. Reichhardt, G. Volpe, and G. Volpe, Reviews of Modern Physics **88**, 045006 (2016).
[26] W. Gao, A. Pei, R. Dong, and J. Wang, Journal of the American Chemical Society **136**, 2276 (2014).
[27] J. R. Howse, R. A. L. Jones, A. J. Ryan, T. Gough, R. Vafabakhsh, and R. Golestanian, Physical Review Letters **99**, 048102 (2007).
[28] W. Tai, P. Zhao, and X. Gao, Science Advances **6**, eabb0310 (2020).
[29] C. Lozano, B. Ten Hagen, H. Löwen, and C. Bechinger, Nature Communications **7**, 12828 (2016).
[30] Q. Ze, S. Wu, J. Nishikawa, J. Dai, Y. Sun, S. Leanza, C. Zemelka, L. S. Novelino, G. H. Paulino, and R. R. Zhao, Science Advances **8**, eabm7834 (2022).
[31] M. Doi and S. F. Edwards, Oxford University Press, Oxford (1988).
[32] G. S. Grest, The Journal of Chemical Physics **145**, 141101 (2016).
[33] H. P. Hsu and K. Kremer, The Journal of Chemical Physics **144**, 154907 (2016).
[34] S. Plimpton, Journal of Computational Physics **117**, 1 (1995).
[35] B. Dünweg and W. Paul, International Journal of Modern Physics C **2**, 817 (1991).
[36] A. E. Likhtman, S. K. Sukumaran, and J. Ramirez, Macromolecules **40**, 6748 (2007).
[37] W. B. Lee and K. Kremer, Macromolecules **42**, 6270 (2009).

[38] N. Iwaoka, K. Hagita, and H. Takano, Journal of the Physical Society of Japan **84**, 044801 (2015).
[39] T. T. Perkins, D. E. Smith, and S. Chu, Science **264**, 819 (1994).
[40] S. Martel, Biomicrofluidics **10**, 021301 (2016).
[41] M. Guix, S. M. Weiz, O. G. Schmidt, and M. Medina-Sánchez, Particle & Particle Systems Characterization **35**, 1700382 (2018).
[42] A. A. Solovev, W. Xi, D. H. Gracias, S. M. Harazim, C. Deneke, S. Sanchez, and O. G. Schmidt, ACS Nano **6**, 1751 (2012).
[43] J. Katuri, X. Ma, M. M. Stanton, and S. Sánchez, Accounts of Chemical Research **50**, 2 (2017).
[44] I. Santiago, Nano Today **19**, 11 (2018).
[45] J. M. Newby, I. Seim, M. Lysy, Y. Ling, J. Huckaby, S. K. Lai, and M. G. Forest, Advanced Drug Delivery Reviews **124**, 64 (2018).
[46] F. Burla, Y. Mulla, B. E. Vos, A. A. Roberts, and G. H. Koenderink, Nature Reviews Physics **1**, 249 (2019).
[47] J. Leal, X. Peng, X. Liu, D. Arasappan, D. C. Wylie, S. H. Schwartz, J. J. Fullmer, B. C. McWilliams, H. D. C. Smyth, and D. Ghosh, Journal of Controlled Release **322**, 457 (2020).
[48] F. Xu, J. M. Newby, J. L. Schiller, H. A. Schroeder, T. Wessler, A. Chen, M. G. Forest, and S. K. Lai, ACS Infectious Diseases **5**, 1570 (2019).
[49] L. Canopoli, F. Coulon, and S. T. Wagland, Science of The Total Environment **698**, 134125 (2020).
[50] B. K. H. Lim and E. S. Thian, Science of The Total Environment **813**, 151880 (2022).
[51] A.-Y. Jee, Y.-K. Cho, S. Granick, and T. Tlusty, PNAS **115**, E10812 (2018).
[52] R. Lino, K. Kinbara, and Z. Bryant, Chemical Reviews **120**, 1 (2020).